Fetal antisense oligonucleotide therapy for congenital deafness and vestibular dysfunction

Lingyan Wang[1,†], J. Beth Kempton[1,†], Han Jiang[1,†], Francine M. Jodelka[2], Alev M. Brigande [1], Rachel A. Dumont[1], Frank Rigo[3], Jennifer J. Lentz[4], Michelle L. Hastings[2] and John V. Brigande [1,*]

[1]Department of Otolaryngology, Oregon Hearing Research Center, Oregon Health & Science University, Portland, OR 97239, USA, [2]Center for Genetic Diseases, Chicago Medical School, Rosalind Franklin University of Medicine and Science, North Chicago, IL 60064, USA, [3]Ionis Pharmaceuticals, Carlsbad, CA 92010 USA and [4]Department of Otorhinolaryngology, Neuroscience Center of Excellence, Louisiana State University Health Sciences Center, New Orleans, LA 70112, USA

ABSTRACT

Disabling hearing loss impacts ∼466 million individuals worldwide with 34 million children affected. Gene and pharmacotherapeutic strategies to rescue auditory function in mouse models of human deafness are most effective when administered before hearing onset, after which therapeutic efficacy is significantly diminished or lost. We hypothesize that preemptive correction of a mutation in the fetal inner ear prior to maturation of the sensory epithelium will optimally restore sensory function. We previously demonstrated that transuterine microinjection of a splice-switching antisense oligonucleotide (ASO) into the amniotic cavity immediately surrounding the embryo on embryonic day 13–13.5 (E13–13.5) corrected pre-mRNA splicing in the juvenile Usher syndrome type 1c (Ush1c) mouse mutant. Here, we show that this strategy only marginally rescues hearing and partially rescues vestibular function. To improve therapeutic outcomes, we microinjected ASO directly into the E12.5 inner ear. A single intra-otic dose of ASO corrects harmonin RNA splicing, restores harmonin protein expression in sensory hair cell bundles, prevents hair cell loss, improves hearing sensitivity, and ameliorates vestibular dysfunction. Improvements in auditory and vestibular function were sustained well into adulthood. Our results demonstrate that an ASO pharmacotherapeutic administered to a developing organ system *in utero* preemptively corrects pre-mRNA splicing to abrogate the disease phenotype.

INTRODUCTION

Thirty-four million children worldwide have disabling hearing loss (http://www.who.int/mediacentre/factsheets/fs300/en/). Permanent congenital and early-onset forms together affect 2–6 neonates per thousand live births with a genetic basis identifiable in 80% of prelingual deafness cases [1,2]. Recent efforts to rescue hearing and vestibular function in murine genetic models of human inner ear disease have exploited strategies based on gene replacement, RNA splicing correction, RNA interference, genome editing, and pharmacotherapeutics [3–17]. Usher syndrome is responsible for 50% of all deaf-blindness cases with 3.2–6.2 individuals affected per 100 000 [18]. The severity of the hearing, vestibular and vision phenotypes predicates clinical classification. Usher syndrome type 1 is the severest form characterized by profound hearing loss or deafness with vestibular dysfunction at birth and the onset of retinitis pigmentosa by early adolescence [19]. There is no medical treatment to prevent or slow progression of Usher syndrome.

Sensory hair cells in the inner ear possess mechanically sensitive ion channels activated by vibrational energy associated with sound and movement [20]. Hair cells convert these stimuli into electrical signals that underlie hearing and vestibular function. Harmonin is a PDZ-domain containing protein that localizes to the upper tip link density of stereocilia and to the ribbon synapse of hair cells [21,22]. Mutations in harmonin affect mechanoelectrical transduction and synaptic transmission [21–23]. The Usher syndrome type 1c knock-in mouse mutant (*Ush1c*) was produced by replacing part of the murine harmonin gene with the *Ush1c c.216A* point mutation that originally arose in type 1C patients in the Acadian community [24,25]. The mutation introduces a cryptic splice site in exon 3 that is used with strong preference over the natural site, leading to

---

*To whom correspondence should be addressed. Tel: +1 503 494 2933; Fax: +1 503 494 0951; Email: brigande@ohsu.edu
†The authors wish it to be known that, in their opinion, the first three authors should be regarded as joint First Authors.

a frameshift and premature stop. Mice homozygous for the human disease allele closely model human USH1C pathogenesis with congenital deafness, vestibular dysfunction by postnatal day 14 (P14), and abnormal electroretinograms at P30 (25).

Antisense oligonucleotides (ASOs) are chemically synthesized polymers consisting of 12–30 nucleotides in length that bind RNA molecules using Watson–Crick base pairing rules (26). Targeted ASOs are designed to modulate gene expression by sterically interfering with pre-mRNA splicing or mRNA translation, or by triggering mRNA catabolism (27). Rescue of hearing and vestibular function in the *Ush1c* mutant has been achieved by neonatal, intraperitoneal injection of a targeted antisense oligonucleotide, ASO-29, that sterically blocks splicing from the cryptic site to restore wild type message and therapeutic levels of harmonin protein (9). Remarkably, ASO-29 must be administered by P5 to optimally rescue hearing, and by P1 to maximally restore vestibular function (10,28). Intervention after these postnatal ages dramatically reduced therapeutic benefits (9,10,28). Similarly, adeno-associated virus (AAV)-mediated gene replacement of harmonin isoform b in the *Ush1c* mutant by inoculation of the cochlea through the round window membrane at P0-P1 restored auditory thresholds and acoustic startle responses, but treatment at P10–12 was ineffective (7). The strict temporal requirements for ASO-29 pharmacotherapy and AAV-mediated harmonin b gene replacement is not an interventional constraint unique to *Ush1c*. AAV-mediated gene replacement of vesicular glutamate transporter 3 (*Vglut3*) in the *Vglut3* knockout mouse produced sustained hearing recovery by inoculation at P1–P3, though inoculation at P10–12 was significantly less effective (3). We define the responsivity of the mouse inner ear to molecular correction at P0–P5 as the early postnatal window of therapeutic efficacy (Figure 1).

Critically, the P0-P5 mouse inner ear is functionally immature and does not respond to sound. Developmentally, the P5 mouse inner ear is equivalent to a human fetal inner ear at gestational week 18 (GA18) (29,30). We hypothesize that the early postnatal window of efficacy defined in the *Ush1c* and *Vglut3* mouse mutants is consistent with an early prenatal window of therapeutic efficacy in humans (31) (Figure 1). These data provide strong rationale to devise and validate fetal gene and pharmacotherapies to treat congenital inner ear disease.

We have previously shown that transuterine microinjection of ASO-29 into the amniotic cavity corrects *Ush1c c.216A* pre-mRNA splicing in the juvenile inner ear (32). Here, we assess the therapeutic benefit of amniotic cavity delivery of ASO and show that harmonin mRNA and protein expression, as well as stereociliary bundle morphology, were significantly improved. However, only marginal improvement in auditory function and partial rescue of vestibular function were achieved. To bypass the anatomical challenges associated with reliably targeting the amniotic cavity earlier than E13–13.5 and to negate the indirect routes of drug entry from the amniotic cavity to the embryo, we microinjected a single dose of ASO-29 through the uterus directly into the fluid-filled cavity of the developing inner ear. We show that a single dose of ASO delivered to the E12.5 otic vesicle rescues hearing and vestibular function

in treated *Ush1c* mutants that is sustained well into adulthood. Our data suggest that fetal pharmacotherapeutics to modulate RNA splicing is an effective strategy to treat congenital deafness and vestibular dysfunction.

MATERIALS AND METHODS

Oligonucleotides

ASO-29 (5′-AGCTGATCATATTCTACC-3′) and ASO-control oligonucleotide (ASO-C; 5′-TTAGTTTAATCA CGCTCG-3′) were synthesized with a fully-modified phosphorothioate backbone and 2′-*O*-methoxyethyl (2′-MOE) modifications at all positions as previously described (9,32). Lyophilized ASOs were dissolved in 0.9% saline, 0.2 μm filtered, quantified by absorbance at 260 nm, and stored at −80°C until use.

Animal husbandry and use

Animal Care Protocol IP000935 governing use of mice was approved by the Institutional Animal Care and Use Committee of Oregon Health & Science University. Mice bearing the causal mutation for human Usher syndrome type 1C (*USH1C c.216G>A*) on the C57BL/6.129S6 background and wild type for the *Cdh23^753G* allele, were expanded as a single colony through more than 10 generations and obtained from Louisiana State University (25). Heterozygous *Ush1c^216GA* females were bred with homozygous *Ush1c^216AA* males to produce mutant and control mice. For timed pregnancies, noon on the day an early morning vaginal plug was detected was designated embryonic day 0.5 of gestation (E0.5). Since fertilization may occur anytime during the 12 h dark cycle, natural variation in embryonic age was up to six pairs of somites. This variation is evident in Supplementary movies S1 and S2 where the embryos were staged to early E12.5 and late E12.75, respectively, with an appropriate difference in otic vesicle morphogenesis observed. The prophylactic analgesia and anesthesia detailed below were administered in strict accordance with the recommendations in the *Guide for the Care and Use of Laboratory Animals* of the National Institutes of Health (33).

Mouse survival surgery and transuterine microinjection

The preoperative, operative, and postoperative procedures for ventral laparotomy are detailed in our previous manuscript (34). Video demonstration of transuterine microinjection into the E12.5 mouse otocyst is presented in Supplementary Movie S1 and in our previous publication (34). Video demonstration of transuterine microinjection into the E13–13.5 mouse amniotic cavity is shown in our previous study (32). ASO-29 and ASO-C (22.4 μM stocks) were mixed with crystalline fast green tracer dye to tinge the ASO solution blue without causing appreciable dilution. A custom-fabricated glass capillary micropipette was produced with an 18–24 μm outer diameter and a 20-degree bevel. Mice were anesthetized with sodium pentobarbital (65–70 mg/kg, Sigma, P3761) and post-procedural pain was managed with the nonsteroidal anti-inflammatory Meloxicam (5 mg/kg, Boehringer Ingelheim). ASOs were microinjected through the uterus into the lumen of the otocyst
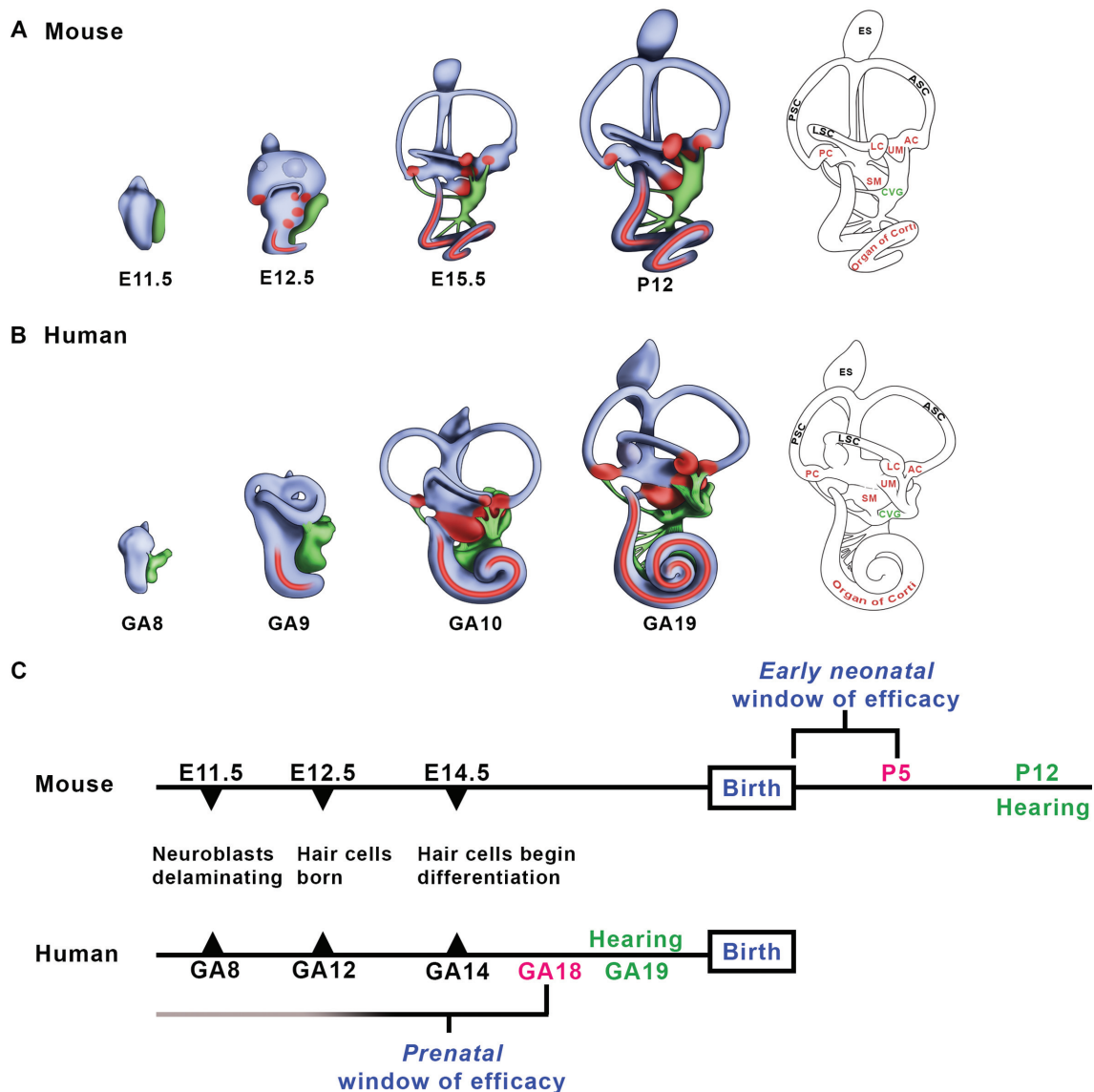
Figure 1. The onset of hearing in the postnatal mouse and the human fetus frames a window of therapeutic efficacy. (A, B) Mammalian inner ear morphogenesis. Lateral view of a right mouse (**A**) and human (**B**) inner ear from the otic vesicle stage to the elaboration of the membranous labyrinth. The onset of hearing defined by positive acoustic startle responses is first present at P12 in the mouse and at 19 weeks gestational age in the human (GA19; weeks since the first day of the last menstrual period) (29,30). Red, auditory and vestibular sensory patches; green, cochleovestibular ganglion. (**C**) Developmental timelines for mouse and human hearing onset. Noted are the approximate embryonic day (E) and weeks gestational age (GA) at which neurons and auditory sensory hair cells are born and differentiate. An early neonatal window of therapeutic efficacy in the mouse is present immediately after birth to P5 (3,6,7,9,10), one week prior to postnatal hearing onset (90). A corollary prenatal window of efficacy in humans is predicted to close by GA18, one week prior to fetal hearing onset (29,30). We hypothesize that fetal gene and pharmacotherapies will be required to achieve optimal restoration of sensory function in human inner ear diseases with congenital or early neonatal onset. Abbreviations: AC: anterior crista; ASC: anterior semicircular canal; CVG: cochleovestibular ganglion; E, embryonic day; ES, endolymphatic sac; LC, lateral crista; LSC, lateral semicircular canal; PC, posterior crista; PSC: posterior semicircular canal, SM, saccular macula; UM, utricular macula.

with a nitrogen-driven Picospritzer III pressure injector on E12.5. The entire lumen of the otocyst was filled until the nascent endolymphatic duct and the cochlear duct were visible (Figure 2A, Supplementary Movie S1). Approximately 200–250 nl (27–34 ng) of ASO was microinjected into one otocyst per embryo. The frequent presence of embryonic resorptions in the C57BL/6.129S6 dams at E12.5 introduced blood into the uterine lumen making intra-otic targeting more challenging than in dams without resorptions. Approximately equal proportions of male and female mice in experimental and control groups were evaluated.

The post-laparotomy C57BL/6.129S6 dams often displayed a propensity for cannibalism and a disinterest in nurturing apparently healthy pups. This problematic maternal behavior interfered with accurate estimates of survival-to-weaning rates for pups having undergone intra-otic ASO-29 delivery at E12.5. However, in our previous study, significantly higher doses of ASO-MALAT1 and a control ASO
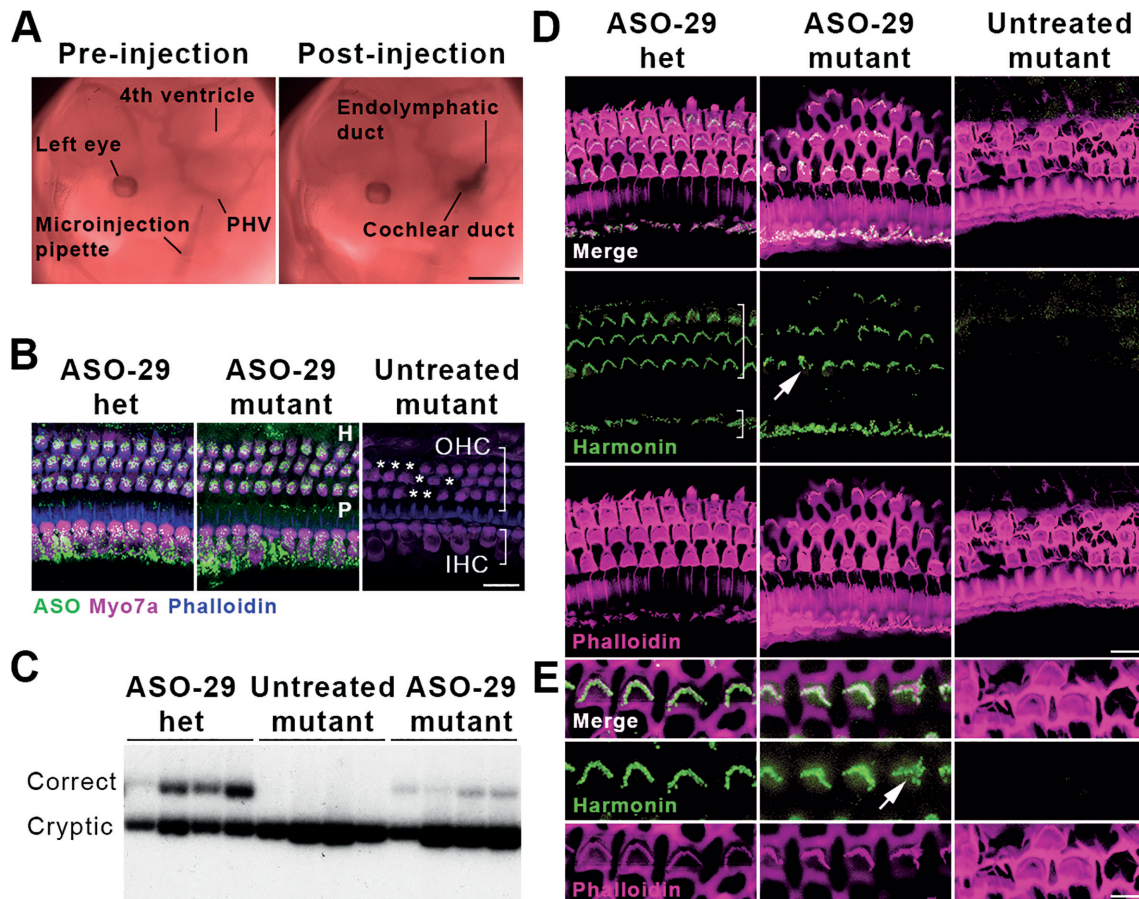
Figure 2. Transuterine microinjection of ASO-29 into the otic vesicle restores harmonin mRNA and protein expression. (**A**) ASO delivery by transuterine microinjection into the lumen of the left otic vesicle is validated by observation of the endolymphatic and cochlear ducts post-injection (compare to Figure 1A, E11.5). PHV: primary head vein. Scale bar: 1 mm. (**B**) ASO-29 localizes to inner hair cells (IHC, short bracket), outer hair cells (OHC, long bracket) as well as the Hensen's cell region (H, lateral to the third row of OHCs) and the pillar cell region (P, in between IHCs and the first row of OHCs) at P30. Asterisks indicate missing OHCs in the untreated mutant. Het: heterozygote. Scale bar: 20 μm. (**C**) Correctly spliced harmonin mRNA was detected in the P30 cochlea of ASO-29-treated heterozygous and mutant mice with a primer set that also detects the cryptically spliced form. (**D**) Harmonin protein expression was observed in stereociliary bundles of IHCs and OHCs of the cochlear apex in ASO-29-treated mutants at P30. Phalloidin labels filamentous actin. Arrow indicates a misshapen bundle in the ASO-29 treated mutant. Scale bar: 10 μm. (**E**) Higher magnification of OHCs showing harmonin expression in the bundles. Arrow indicates a misshapen bundle in the ASO-29 treated mutant. Scale bar: 5 μm. Fluorescent images are representative of $n = 3$ per treatment group in (B), (D) and (E). For splicing assessment, $n = 4$ per group in (C).

delivered to the amniotic cavity of E13–13.5 conceptuses carried a 94% survival rate, suggesting that an ASO with similar chemistry is not grossly teratogenic (32).

In vivo ASO-29 dose response

Four ASO-29 concentrations (1.9, 9.5, 15.2 and 19.0 μM) were tested for efficacy by assessing P30 auditory thresholds at four test frequencies (Supplementary Figure S1). ASO-29 at 19.0 μM (∼27–34 ng ASO delivered) was the highest drug concentration whose viscosity permitted reliable transuterine microinjection into the otic vesicle. ASO-29 at 19.0 μM generated the most robust auditory recovery and this concentration was used throughout the study (Supplementary Figure S1).

RT-PCR analysis of splicing

Inner ears were rapidly dissected and immediately frozen in liquid nitrogen. Tissue was stored at −80°C until ship-ment on dry ice from Oregon to Illinois. RNA was isolated using Trizol reagent and one microgram was reverse transcribed using GoScript Reverse Transcriptase (Promega, Fitchburg, WI, USA). One microliter of cDNA was used in PCR reactions with GoTaq Green (Promega) supplemented with primers and α-32P-dCTP. Reactions were heated at 95°C for 2 min, followed by 37 cycles of: 95°C denaturation for 30 s, 58°C annealing for 30 s, 72°C extension for 1 min, and a final extension at 72°C for 2 min. Primers specific for mouse exon 2 (5′-CTCATTGAAAATGACGCAGAGAAGG-3′ and mouse exon 5 (5′-TCTCACTTTGATGGACACGGTCTTC-3′) were used to amplify cDNA generated from both the wild-type mouse Ush1c allele and the Ush1c allele with the mutated human USH1C insertion (*USH1C c.216G>A*). Products were separated on a 6% non-denaturing polyacrylamide gel and quantitated using a Typhoon 9400 phosphorimager (GE Healthcare). The amount of correct *Ush1c* splicing was quantified and presented as the percent of total *Ush1c* mRNA that is correctly spliced [(correctly spliced

products/(correctly spliced products + cryptically spliced products) $\times$ 100].

Immunofluorescence

ASO: All the steps were performed at 22°C except where otherwise noted. Triplicate, 5 min washes were performed in calcium-free phosphate buffered saline (PBS; in mM: 137 NaCl, 2.7 KCl, 9.9 Na_2HPO_4, 2 KH_2PO_4, pH 7.2) with gentle agitation. Inner ears were grossly dissected by separation from the temporal bone and removal of the bulla with associated connective tissue. Grossly dissected inner ears were fixed in 2% paraformaldehyde in PBS for 2 h at 4°C with gentle agitation. After overnight decalcification in 10% ethylenediaminetetraacetic acid (EDTA) pH 7.2, the inner ears were microdissected and immersed in Image IT (Invitrogen) for 30 min; permeabilized for 2 h in 10% normal goat serum, 0.5% bovine serum albumin (BSA), 0.03% saponin, and 0.1% Triton X-100 in PBS; incubated for 2 h at 4°C with primary antibodies (rabbit anti-ASO, 1:500 from Ionis Pharmaceuticals [32] and mouse anti-Myosin 7a clone 138-1, 1:500 from Developmental Studies Hybridoma Bank) in 3% normal goat serum (Invitrogen), 0.5% BSA, 0.03% saponin, and 0.1% Triton X-100 in PBS; and then incubated for 2 h at 4°C with anti-rabbit IgG-conjugated Alexa Fluor 488 and anti-mouse IgG-conjugated Alexa Fluor 568 at a dilution of 1:300 (Molecular Probes, Eugene, OR, USA). Whole-mount organs of Corti were labeled by a 1:150 dilution of Alexa Fluor 660-conjugated phalloidin for 30 min (Molecular Probes).

Harmonin:Harmonin expression was detected by an antigen retrieval technique as previously described (35). Grossly dissected inner ears were initially fixed in 4% paraformaldehyde in PBS for 10 min, secondarily fixed and permeabilized in a 1:1 mixture of methanol and acetone for 10 min at −20°C, and washed in PBS. Microdissected inner ears were permeabilized in 0.5% Triton X-100 and 10% normal goat serum (Invitrogen Life Sciences) for 1 h, incubated overnight at 4°C in a 1:200 dilution of rabbit anti-harmonin H3 primary antibody (22) (gift from Peter Barr-Gillespie), and then incubated overnight at 4°C in a 1:300 dilution of anti-rabbit IgG-conjugated Alexa Fluor 568. Hair bundle morphology was revealed by a 1:150 dilution of Alexa Fluor 488-conjugated phalloidin for 30 min.

Myosin7a: Five microdissected whole cochleae from each treatment group were permeabilized and blocked in blocking solution consisting of 3% goat serum, 1% BSA and 0.2% saponin. A 1:100 dilution of rabbit Myosin7a (Proteus Biosciences Inc., Ramona, CA, USA) was applied in blocking solution overnight at 4°C with gentle agitation. A 1:150 dilution of anti-rabbit IgG-conjugated Alexa Fluor 568 was applied in blocking solution for 2 h. Filamentous actin was labeled by a 1:150 dilution of Alexa Fluor 660-conjugated phalloidin for 30 min. Immunostained cochleae were mounted in VectaShield (Vector Laboratories, Burlingame, CA, USA) and imaged with an Olympus FV1000 laser-scanning confocal microscope.

Cochlear place-frequency map and hair cell quantitation

The number of Myosin7a positive hair cells along the tonotopic axis was counted in 200 μm arcs at eight basilar mem-

brane positions from 0.5 mm to 4.0 mm from the apex in 0.5 mm steps (36,37). The correlative cochlear place-frequency map was based on the equation $d\ (\%) = 156.5 - 82.5 \times \log(f)$, where d is the normalized distance from the base (%) and f is the frequency in kHz (38). The denominator in the normalization distance from the base calculation uses an average adult CBA mouse tonotopic axis length of 5.13 mm measured along the neural edge of the organ of Corti just beneath the inner hair cells. See Supplementary Figure S2 for whole mount immunofluorescence and SEM representations of the mouse place-frequency map used in this study.

Scanning electron microscopy (SEM)

SEM samples were prepared with the following modifications of a published protocol (39). Mouse temporal bones were removed and submerged in 4% paraformaldehyde for 4 h at 4°C. The inner ear was dissected away from the temporal bone and a small hole was introduced into the apex of the cochlea with Biologie #5 forceps (Fine Science Tools) to allow fixative to fully penetrate the tissue. The inner ear was decalcified in 10% EDTA overnight at 4°C. The sensory epithelium was exposed by removal of the lateral wall and the tectorial membrane with Biologie #5 forceps and iridectomy scissors. The tissue was transferred to 2.5% glutaraldehyde in 0.15 M cacodylate buffer, pH 7.4 at 4°C for 12 h. The tissue was then subjected to an osmium-thiocarbohydrazide procedure (OTOTO), alternating through three 1 h osmium tetroxide incubations interspersed with two 20 min 1% thiocarbohydrazide incubations (40). The tissue was dehydrated by an ethanol series and critical point dried (K850, Quorum Technologies) with liquid CO_2. Samples were mounted on adhesive tabs (Electron Microscopy Sciences) and imaged using an FEI Sirion XL30 FEG field-emission scanning electron microscope operated at 5 kV.

Stereociliary bundle quantitation

The percentage of OHCs with intact stereociliary bundles or atypical bundles was quantified by SEM at 1.0, 2.0 and 3.0 mm from the cochlear apical tip in 120 μm arcs defined with NIH ImageJ (version 1.51).

Auditory brainstem response (ABR)

Acoustic stimuli were digitally generated and auditory responses were monitored using a National Instruments PXI stimulus generation/data acquisition system that included a 24 bit digital DAQ board (PXI-4461) and a 16 bit DAQ board (PXI-6221) and the Eaton Peabody Laboratory Cochlear Function Test Suite. To elicit the ABRs, 5-ms tone pip stimuli were generated with 0.5-ms rise/fall times (cosine squared) in alternating polarity at 30/s. Acoustic stimuli were delivered via a custom acoustic assembly comprising two dynamic drivers as sound sources and a miniature electret microphone to measure sound pressure *in situ*. The response from the electrodes was amplified (10 000×), filtered (300 Hz–3 kHz bandpass), and averaged (300 samples) at each frequency-level combination.

Animals were anesthetized with a cocktail of ketamine (60 mg/kg; Hospira, Inc.), xylazine (6 mg/kg;

AnaSed, Lloyd Laboratories) and acepromazine (1 mg/kg; Boehringer Ingelheim). Responses were collected with a subcutaneous recording needle electrode at the vertex, a reference electrode ventrolateral to the pinna of the test ear, and a ground in the ipsilateral forepaw. ABRs were recorded at 8, 16, 24 and 32 kHz. Sound level was incremented in 5 dB steps, from ∼10 dB below threshold to ∼30 dB above threshold with a limit of 85 dB SPL as the loudest intensity presented. Threshold for ABRs was defined as the lowest stimulus level at which a repeatable response from two of the five waves could be identified above the noise floor in the response waveform. Threshold scoring was accomplished using ABR Peak Analysis program (version 1.0.0.6).

Distortion product otoacoustic emission (DPOAE)

DPOAEs were recorded for primary tones (f1, f2) with a frequency f2/f1 ratio of 1.2. The f2 primary was presented at 8, 12, 16, 24 and 32 kHz from 20 to 70 dB SPL, incremented in 10 dB steps with the level of the f2 primary 10 dB less than the f1 level. Ear canal sound pressure was amplified and digitally sampled, Fourier transforms were computed and averaged, and the 2f1-f2 DPOAE and surrounding noise floor were extracted. Data were graphed and statistically compared at the f2 stimulus level of 60 dB SPL.

Acoustic startle reflex responses

Acoustic startle responses were measured in the SR-LAB startle response system (San Diego Instruments). The mice were acclimatized to the darkened startle chamber by a 4 min presentation of 65 dB white noise from a speaker mounted 24 cm above the support platform. Startle stimuli of 40 ms duration and 2 ms rise/fall times at 80, 90, 100, 110 and 120 dB were presented in pseudo-random order generated with varying inter-trial intervals of 10–30 s. Each stimulus was presented 8 times. A piezoelectric accelerometer sealed to the underside of the animal support platform recorded the movement for 65 ms after onset of the stimulus. Average peak startle amplitude within the first 20 ms was calculated at each sound intensity using SR-LAB analysis software (6300-000-K).

Open field behavior

A mouse was placed in an open plastic cage (26 cm × 15.5 cm) and its movement was recorded with a Sony HDR-CX675 camcorder. The digital video file was imported and saved in native m2ts format with PlayMemories Home software (Sony, version 5.4.02.06120). The footage was then trimmed to 120 seconds with Adobe Premiere Pro CC (version 2017.0.1). Video was exported in MP4 format with H.264 2-pass VBR encoding (1280 × 720, 29.97 frames per second, 12 mbps bitrate). Movement was analyzed with EthoVision XT software (Noldus, version 13.0.1216). Arena calibration was based on the manually-specified lengths of all four sides of the cage. Automatic tracking was performed with detection of the nose-point, center-point, and tail-base. Distance traveled (cm/120 s), average velocity (cm/s), and frequency of 360° rotations (number/120 s) were computed based on the position of the nose-point.

Musculoskeletal coordination testing

Rota-Rod testing is significantly influenced by the vestibular system (41). Mice were placed in individual lanes on the Rota-Rod apparatus (Omnitech Electronics, Inc.) at a baseline rotation of 4 RPM and then accelerated at a constant rate to 40 RPM over the course of 240 s. Three trials per mouse separated by at least a 20 min rest period were recorded and the average latency to fall (seconds) was calculated. Mice had previously been acclimated to the Rota-Rod testing paradigm by using the same constant acceleration protocol for two sessions in the three to four days prior to the experimental run that was quantified. During acclimation, up to three falls were allowed per mouse per trial.

Swim test

Swimming was evaluated by recording digital video of a mouse gently set into a clear plastic container (35 × 30 cm) filled with 37°C water. A wild-type mouse swims by keeping its nose above the surface of the water, paddling with all four paws, and moving the tail in an S-shaped pattern to translocate briskly toward the side of the container (42). A swim score from 0 to 2 was assigned based on the ability to swim, with 0 indicating barrel-rolling and/or submarining and thus an inability to swim (in which case the test was stopped immediately and the subject recovered); 1 indicating swimming with uncoordinated movements; and 2 indicating brisk translocation on the water's surface (28).

Reaching test

The reaching reflex was evaluated by holding the tail and lowering the mouse toward a solid surface (43). Mice with impaired vestibular function do not sense gravitational forces correctly and curl toward their tails frequently, but wild-type mice stretch their paws out toward the solid surface to support touch down. Digital video was manually analyzed in slow motion with EthoVision XT to determine the frequency of nose translocations that breeched the shoulder line (i.e., reaching caudally) per trial.

Statistical analyses

All statistical tests were run in GraphPad Prism v 7.04. Splice correction was analyzed employing a one-tailed t-test to evaluate the increase in the percentage of correctly spliced full length *Ush1c* mRNA in the ASO-29-treated mutant and the ASO-29-treated heterozygote compared to the untreated mutant. Additionally, the ASO-29-treated mutants and heterozygotes were compared by a two-tailed *t*-test. Inner and outer hair cell counts were analyzed by a repeated measures two-way ANOVA with Tukey's multiple comparison post-hoc test.

To statistically analyze ABRs, ears with no response at 85 dB SPL were assigned a value of 90 dB SPL. This was a conservative threshold estimate since the sound level was incremented in 5 dB steps. To determine normality of data, histograms were generated for each of the ABR frequencies tested within all groups. In addition, the Shapiro–Wilk test to interrogate normality was conducted. It was determined, based on these results, that the assumption of normalized data had not been met in all groups. Therefore,

the Kruskal–Wallis non-parametric one-way ANOVA test was run at each ABR frequency. Dunn's multiple comparison test was used for post hoc comparisons of the mean rank differences between the mutant groups, the heterozygote groups, and mutants versus heterozygotes.

Statistical analysis of DPOAEs was carried out at f2 stimulus level of 60 dB SPL. Tests of normality were conducted as above and normalized data were rejected. Kruskal–Wallis non-parametric one-way ANOVA test was employed at each frequency with Dunn's multiple comparison post-test.

Statistical analysis of startle responses was performed by repeated measures two-way ANOVA with Dunnett's multiple comparison post-hoc test comparing all groups to the untreated mutant group at each intensity level. Distance traveled, velocity, 360° rotations, latency to fall, swim scores, and nose translocations past the shoulder line were analyzed by one-way ANOVA with Tukey's multiple comparison post-hoc test.

RESULTS

Amniotic cavity ASO administration sub-optimally improves hearing and vestibular function

ASOs do not appreciably cross the maternal-placental interface (44)(unpublished data). We reasoned that an effective fetal pharmacotherapeutic strategy must present bioactive quantities of ASO-29 to otic epithelial progenitor cells in the *Ush1c* mutant inner ear prior to endogenous harmonin expression and functional maturation of hair cells. In an initial study validating the utility of fetal pharmacotherapeutics to modulate pre-mRNA splicing, we showed that 100 μg of ASO-29 microinjected into the amniotic cavity at E13–13.5 corrected *Ush1c c.216A* splicing in the cochlea of P22 *Ush1c* mutant mice to a similar level as the splicing correction observed with an intraperitoneal injection of ASO-29 at P5 (9,32). Here, we further assessed the therapeutic efficacy of amniotic cavity delivery and found that harmonin expression in the stereociliary bundles of cochlear hair cells was restored, hair cell survival was enhanced, bundle morphology was stabilized, and partial rescue of vestibular behavior was observed (Supplementary Figure S3). However, this delivery paradigm at the tested dose resulted in only marginal improvement in auditory function (Supplementary Figure S3).

Otic vesicle ASO administration corrects harmonin splicing in the adult Ush1c mutant inner ear

We initially considered intra-amniotic cavity injections at E11–12 in an effort to dose the embryo earlier than E13–13.5 but the propensity for leakage outside the amniotic cavity at these stages made reliable ASO dosing problematic (data not shown). We next considered ASO presentation directly to the *Ush1c* mutant inner ear prior to E13–13.5 (Supplementary Figure S4 and Supplementary Movie S1). Fortuitously, the otic vesicle stage of mammalian inner ear development presents a teardrop-shaped, fluid-filled structure lined with progenitor cells that give rise to hair cells, supporting cells, and the neurons that innervate the inner

ear (Figure 1A,B) (45,46). We postulated that the embryonic day 12.5 (E12.5) otic vesicle might serve as a suitable biological reservoir of sufficient volume to deliver therapeutic quantities of ASO-29 and restore sensory function postnatally. We microinjected ASO-29 or a non-targeting ASO control (ASO-C) into the lumen of the E12.5 otic vesicle by transuterine microinjection (Figure 2A, Supplementary Movie S1) (34,47). Optimal vesicle targeting was confirmed by the observation of vesicle swelling during the injection of ASO-29 and clear definition of the endolymphatic and cochlear ducts post-injection (Figure 2A and Supplementary Movie S1).

To determine if microinjection of ASO-29 into the fetal inner ear leads to detectable levels of drug in the sensory epithelium of the mature, adult inner ear, cochlear whole mount immunofluorescence was performed at P30 using an antiserum against the ASO (32). ASO-29 was robustly detected in myosin 7a (Myo7a)-labeled inner and outer hair cells (IHC and OHC), Hensen's cells (H), and inner and outer pillar cells (P) of treated heterozygous and mutant mice (Figure 2B). ASO-29 was detected only sporadically in other cells in the inner ear.

No fluorescent signal was detected in cochleae from untreated *Ush1c* mutants indicating the absence of nonspecific antibody binding (Figure 2B, Untreated mutant). Consistent with the detection of ASO-29 in IHCs and OHCs, correctly spliced harmonin mRNA was detected in all four ASO-29 treated *Ush1c* P30 cochleae examined (Figure 2C). The percentage of correctly spliced *Ush1c* mRNA in ASO-29-treated mutants and heterozygotes was 4.84 ± 1.61 and 28.7 ± 5.14, respectively ($P < 0.05$, two-tailed Student's t-test). No correctly spliced harmonin mRNA was detected in untreated mutants. Importantly, the percentage of splicing correction achieved by intra-otic administration of ASO-29 at E12.5 did not rise to wild type splicing levels but was comparable to the levels achieved by amniotic cavity delivery (32) and by intraperitoneal injection of ASO-29 into neonates at P3–P5 (9). In summary, the splicing correction data suggest that intra-otic injections of ASO-29 may also support therapeutic levels of wild type *Ush1c* mRNA synthesis in the adult cochlea.

Harmonin protein expression is restored in the stereociliary bundle of ASO-treated *Ush1c* mice

To assess harmonin protein expression in stereociliary bundles of ASO-29-treated mutants, whole mount immunofluorescence was conducted at P30 (Figure 2D, E). The distribution of harmonin in ASO-29-treated mutant IHCs and OHCs was similar to that of ASO-29-treated heterozygotes (Figure 2D, ASO-29 het and ASO-29 mutant). Harmonin was undetectable in untreated mutants (Figure 2D,E). Intriguingly, the ASO-29-treated mutant mice appeared to have a full complement of IHCs and OHCs in their stereotyped row distributions (Figure 2D) compared to untreated mutants that displayed OHC loss characteristic of the *Ush1c* mutation (Figure 2B, asterisks) (7,9).

Hair cell survival is enhanced in ASO-treated *Ush1c* mice

To rigorously quantify the ASO-29 effect on hair cell survival, Myo7a-labeled hair cells were counted in represen-

tative regions along the tonotopic axis 0.5–4 mm from the cochlear apical tip (8–32 kHz inclusive) (Figure 3 and Supplementary Figure S2A). The number of IHCs and OHCs in ASO-29-treated mutants compared to heterozygotes was not significantly different at any cochlear location other than for OHCs at 4 mm ($P < 0.05$), indicating that ASO-29 preserved wild-type numbers of auditory hair cells (Figure 3B). Importantly, ASO-29-treated mutants displayed increased IHC counts at 1–2 mm and at 3 mm from the cochlear apical tip compared to untreated mutants (Figure 3B). Similarly, OHC counts were improved at all of the cochlear locations assessed in ASO-29-treated mutants compared to untreated mutants (Figure 3B).

Stereociliary bundle morphology is improved in ASO-treated *Ush1c* mice

To evaluate hair cell morphology, scanning electron microscopy was conducted at 1, 2 and 3 mm from the apical tip of the P30 cochlea, corresponding to 8–24 kHz sensitivity (Figure 4A, Supplementary Figure S2B). The majority of OHC bundles in ASO-29-treated mutants were grossly intact and approximated the V- or W-shape characteristic of wild-type bundles (Figure 4A). Misshapen and discontinuous stereociliary bundles, however, were observed in the treated mutants (Figure 4A and Figure 2D, E, arrow and arrowheads). All of the ASO-29 treated mutant OHCs sampled 1 mm from the apex displayed bundles and <4% were morphologically atypical (Figure 4B). While 98.5% and 95.7% of OHCs displayed bundles at 2 and 3 mm, respectively, the percentage of atypical bundles in these locations was increased to 17.7% and 40.7%. By contrast, untreated mutants presented progressive loss of OHC bundles from 1 to 3 mm from the apical cochlear tip (13.0–37.7%) with 77–84% of bundles atypical (Figure 4B). In summary, transuterine microinjection of ASO-29 into the E12.5 otic vesicle localized ASO to hair cells and supporting cells in the mature cochlea; enabled wild type harmonin RNA splicing; enhanced harmonin protein expression in stereociliary bundles; preserved IHC and OHC numbers to wild type levels; and improved stereociliary bundle morphology.

Hearing sensitivity is rescued by fetal, intra-otic administration of ASO

To assess auditory function in treated *Ush1c* mutants, hearing sensitivity was measured by auditory brainstem response (ABR) testing at P30. ABR waveforms at 8 kHz from representative mice showed ASO-29-treated mutant responses that were nearly indistinguishable from those of the ASO-29-treated heterozygote (Figure 5A,B). By contrast, ASO-C-treated or untreated mutants were effectively deaf (Figure 5C,D). Remarkably, ASO-29-treated mutants presented significantly improved ABR thresholds at 8, 16 and 24 kHz (Figure 5E–G). These data show that fetal ASO pharmacotherapy restores hearing in the *Ush1c* mutant mouse.

The ABR thresholds for the 30 treated mutant mice ranged from 20 to 85 dB SPL (Figure 5E-H) and we focused on understanding the *in vivo* biological variability of the pharmacotherapeutic response. We defined a dose response relationship between ASO-29 and auditory threshold responses from 1.9 to 19 μM (Supplementary Figure S1). The steepness of the dose response curve suggested that small variations in the amount of ASO-29 delivered has a dramatic effect on hearing recovery. Intrinsic to the transuterine microinjection procedure is the unavoidable leakage of ASO-29 injectate out of the otic vesicle along the path formed by the retracted microinjection pipette (Supplementary Movie S2). This limitation likely contributes to the biological variability we observed. We examined the top-performing quartile of treated mutants reasoning that ASO leakage was minimized in these ears. The average ABR thresholds of the top-performing quartile of ASO-29-treated mutant mice at 8, 16 and 24 kHz were 34 ± 3.2, 53 ± 5.1 and 46 ± 7.4 decibels sound pressure level (dB SPL) at P30 (Figure 5I). High frequency threshold recovery is typically the most difficult to secure, and the top-performing quartile displayed an elevated but improved average threshold at 32 kHz of 70 ± 4.6 dB SPL (Figure 5I).

Sensitive hearing thresholds persist into adulthood

The persistence of auditory recovery is a critical measure of efficacy, and the ASO-29 treatment preserved 8 kHz thresholds within a 21 dB SPL range through 220 days (Figure 5J). Critically, 8 kHz thresholds in the top-performing quartile were sustained from 26 to 38 dB SPL through 220 days (Figure 5J). Similarly, auditory recovery in the top-performing quartile at 16 and 24 kHz was also maintained (Supplementary Figure S5). ABR waveforms at 30, 120 and 220 days from an ASO-29-treated mutant in the top-performing quartile further illustrate the magnitude and persistence of the auditory recovery at the four frequencies tested (Supplementary Figures S6–S8).

Auditory recovery was also assessed in treated *Ush1c* mutants at P30 by distortion product otoacoustic emissions (DPOAE) testing which measures cochlear nonlinearity, a property that is closely influenced by OHC function (48). DPOAE responses of the top-performing quartile of ASO-29-treated mutants to an f2 stimulus of 60 dB SPL at 8, 12 and 16 kHz were improved at 8.4 ± 1.1, 9.5 ± 1.6, 12.3 ± 2.6 dB SPL compared to untreated mutants, respectively. Lastly, we determined whether the rescued hearing was beneficial to treated animals by measuring acoustic startle reflex responses. Impressively, treated mutant mice displayed startle responses that were significantly improved compared to untreated mutants suggesting that appropriate behavioral responses to brief intense sound were partially restored (Figure 5L). In summary, the ASO-29-treated mutants displayed rescued auditory thresholds that are sustained longitudinally; improved DPOAE responses at lower frequencies; and improved acoustic startle reflex responses.

Vestibular function is rescued and sustained into adulthood

To assess vestibular recovery in treated *Ush1c* mutants, equilibrium was measured by open field behavior, musculoskeletal coordination, swimming, and reaching. Ac-
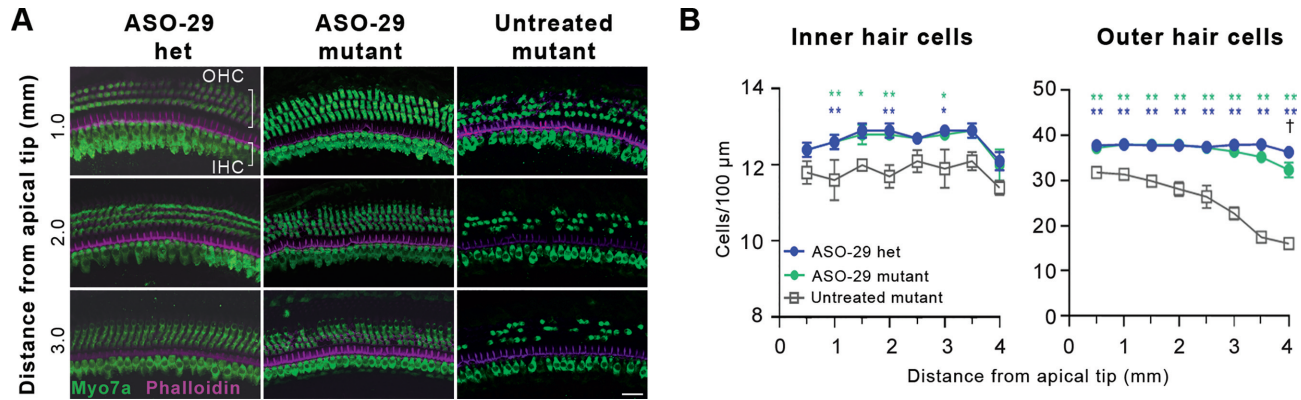
Figure 3. ASO-29 enhances inner and outer hair cell survival. (**A**) Representative whole mount Myosin7a (Myo7a) confocal microscopic projections showing enhanced hair cell survival at 1.0, 2.0 and 3.0 mm from the tip of the cochlear apex (8–24 kHz inclusive) in ASO-29-treated mutants at P30. Distance from the apical tip was translated to frequencies using the cochlear place frequency map shown in Supplementary Figure S2A. Scale bar: 20 μm. (**B**) Quantification of IHCs and OHCs ± SEM 0.5 to 4 mm from the tip of the cochlear apex (8–32 kHz inclusive). Untreated mutants were compared to the two ASO-29 treatment groups by two-way repeated measures ANOVA with Tukey's Multiple Comparison Test: $*P < 0.05$, $**P < 0.01$, $n = 5$ per group. The number of outer hair cells in ASO-29 mutants and ASO-29 heterozygotes was significantly different only at 4 mm by two-way repeated measures ANOVA with Tukey's Multiple Comparison Test: $^{\dagger}P < 0.05$, $n = 5$ per group.
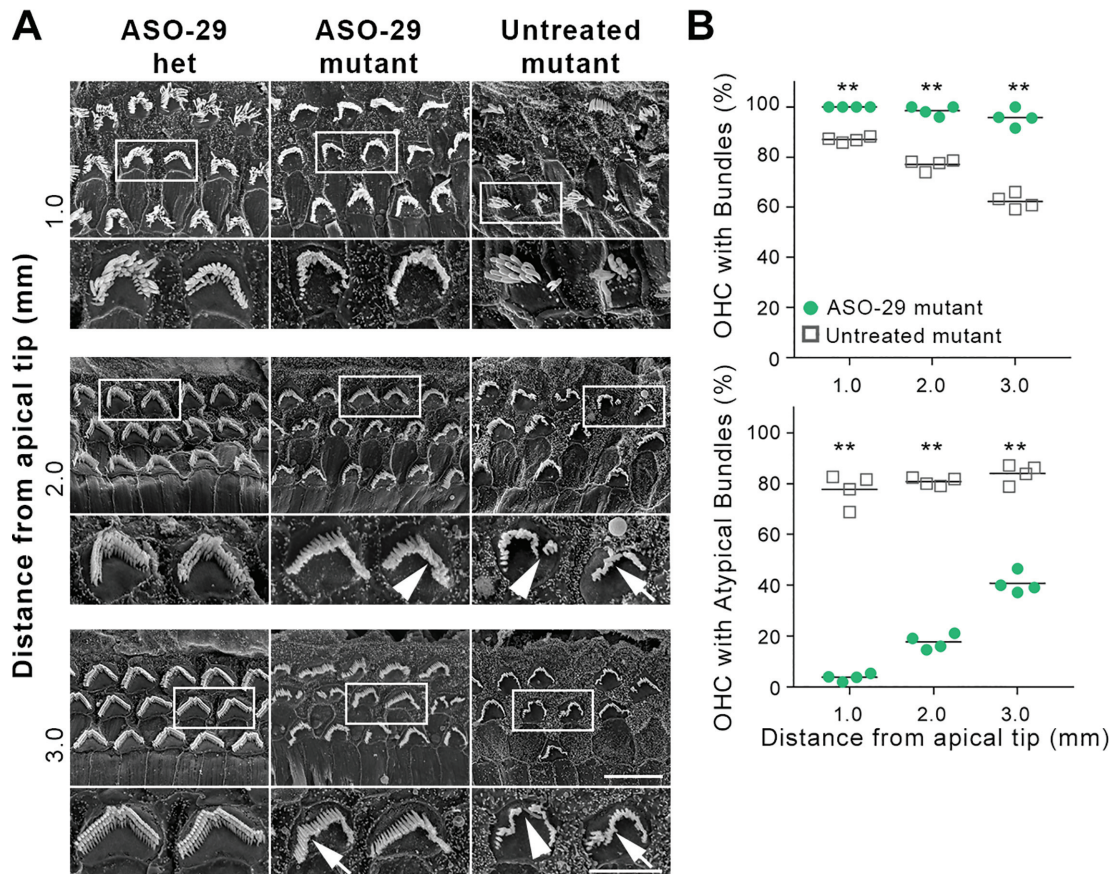
Figure 4. ASO-29 treatment improves outer hair cell stereociliary bundle morphology. (**A**) OHC stereociliary bundle morphology is improved in ASO-29-treated mutant inner ears 1.0, 2.0 and 3.0 mm from the tip of the cochlear apex (8–24 kHz inclusive) at P30. White boxes indicate the bundles shown in the subjacent high magnification panels. Arrows indicate misshapen bundles. Arrowheads indicate discontinuous bundles. Scale bars: 5 μm and 10 μm for the high and low magnification panels, respectively. (**B**) The percentage of OHCs with stereociliary bundles and with atypical bundles in ASO-29 treated mutant cochlea and untreated mutant cochleae at P30. Bundle presence and morphology were scored in 120 μm arcs from scanning electron micrographs taken at 1, 2 and 3 mm (8–24 kHz inclusive) from the tip of the cochlear apex. An atypical bundle displayed waviness or discontinuity as shown in panel (A). A total of 595 and 629 OHCs were scored in 4 ASO-29 treated mutants and four untreated mutants, respectively ($**P < 0.01$; two-tailed unpaired *t*-test).
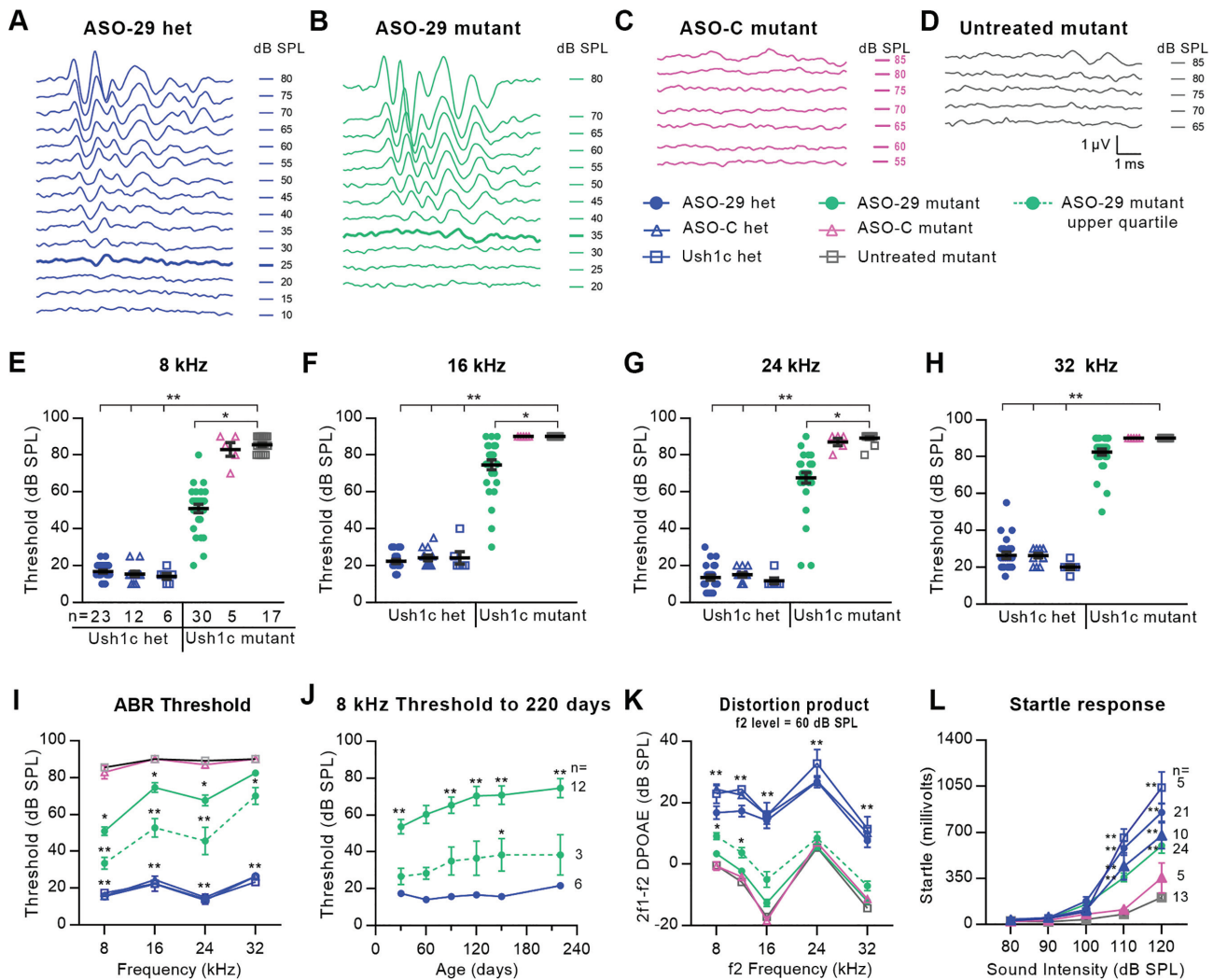
Figure 5. ASO-29 rescues behaviorally-relevant auditory function that is sustained longitudinally. (**A–D**), ABR waveforms at 8 kHz from a representative of each of the four treatment groups. ABR thresholds are indicated by the thickened traces in (A) and (B); no thresholds were detected in the ASO-C treated mutant or the untreated mutant in (C) and (D). (**E–H**) Individual ABR thresholds at the four frequencies tested for every animal in the six treatment groups at P30. (I) ABR thresholds ± SEM for the cohorts in (E–H). The dotted line shows the average ABR thresholds ± SEM for seven ASO-29-treated animals in the upper (top-performing) quartile. (**J**) ABR thresholds ± SEM for 12 ASO-29-treated mutants followed through 220 days. Average thresholds for the upper quartile (*n* = 3) are significantly different from treated heterozygotes only at 140 days. (**K**) Distortion product otoacoustic emission (DPOAE) responses to an f2 stimulus of 60 dB SPL across frequencies ± SEM. The dotted line shows the average of 7 ASO-29-treated animals in the upper quartile (same subjects as in 5I, dotted line). *n* values in (E) apply to panels (F–I) and (K). (**L**) Acoustic startle reflex responses ± SEM. Statistical tests: panels (E–I) and (K): Kruskal–Wallis *H* Test with Dunn's Multiple Comparison Test comparing all groups to untreated *Ush1c* mutant; panel (J): repeated measures two-way ANOVA with Dunnett's Multiple Comparison Test comparing ASO-29-treated mutants to ASO-29-treated heterozygotes. (L), same as (J), but comparing all groups to untreated *Ush1c* mutant. *$P < 0.05$ and **$P < 0.01$. Level of significance for the comparisons involving each of the three heterozygous control groups is $P < 0.01$ and represented by a single asterisk pair in (I) and (K) (**) to reduce the visual complexity of the graph.

tivity traces from representative mice show that ASO-29-treated mutants appropriately preferred the periphery of their cages, traveled similar distances at the same average velocity, and rarely circled compared to ASO-C-treated or untreated mutants (Figure 6A–G, Supplementary Movie S3). Moreover, ASO-29-treated mutant mice balanced on an accelerating, rotating rod; swam; and reached with equal skill compared to the three heterozygous control groups (Figure 6H–J, Supplementary Movie S4 and S5). Significantly, ASO-29-treated mutants sustained wild-type vestibular behaviors through 6 months of age, the latest age tested (Supplementary Figure S9).

DISCUSSION

Our previous work demonstrated that ASO-29 delivery to the E13–13.5 amniotic cavity modulates *Ush1c* pre-mRNA splicing in the cochlea of juvenile *Ush1c* mutant mice (32). The sub-optimal recovery of hearing and vestibular function in treated *Ush1c* mutants drove efforts to deliver ASO-29 directly to the developing inner ear at an earlier stage to effect splicing correction in auditory progenitors and nascent vestibular hair cells prior to endogenous harmonin expression and bundle morphogenesis. Reliable amniotic cavity injections were prohibitive at earlier embryonic stages due to the propensity for leakage outside the restricted vol-
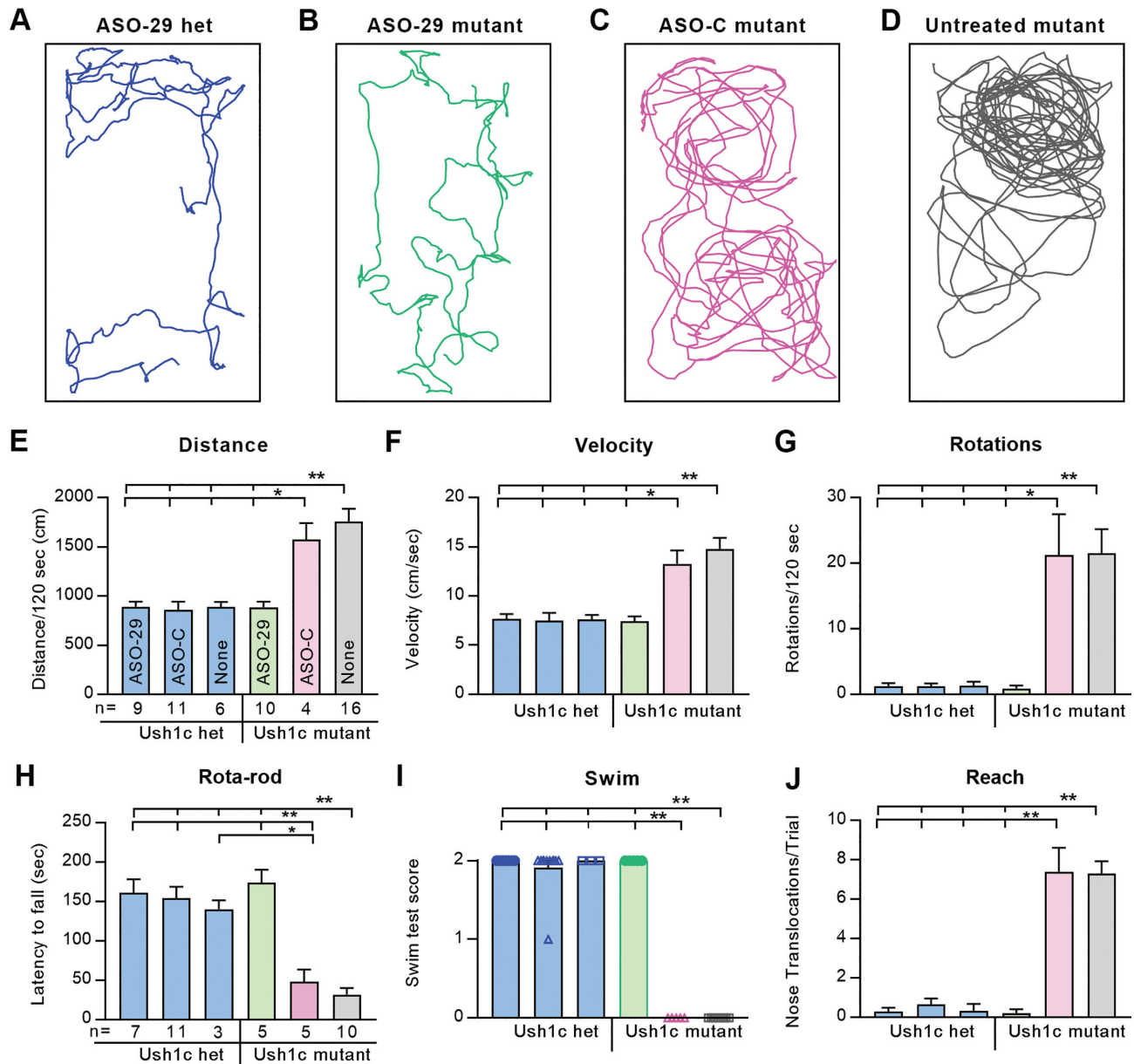
Figure 6. ASO-29 rescues behaviorally-relevant vestibular function that is sustained longitudinally. (**A–D**) Thirty second activity traces from a representative of each of the four treatment groups. (**E–J**) Graphs show average values ± SEM for: (E) distance traveled; (F) average velocity; (G) number of 360 degree rotations; (H) latency to fall; (I) swim score (individuals were plotted so that the zero scores of ASO-C and untreated mutants are readily detected on the X-axis); (J) average number of nose translocations past the shoulder line per trial (i.e., reaching caudally). One-way ANOVA with Tukey's Multiple Comparison Test; **$P < 0.01$ with comparisons indicated by the hatched bars above each panel. *n* values in (E) apply to (F) and (G); *n* values in (H) apply to (I) and (J). The 180 day vestibular function test data are presented in Supplementary Figure S9.

ume of the cavity. To overcome this limitation, we microinjected ASO-29 directly into the otic vesicle at E12.5. This approach bypasses the undefined pharmacokinetics predicated by amniotic cavity delivery and introduces the splice switching ASO directly to the epithelial layer of the inner ear 1–1.5 days earlier than the E13–13.5 amniotic cavity injections. Our data demonstrate that ASO-29 delivered into the E12.5 mouse otic vesicle corrects RNA splicing and enhances harmonin protein expression in sensory hair cells at P30 and rescues auditory thresholds and vestibular function in the *Ush1c* mutant mouse well into adulthood.

The magnitude and persistence of the auditory and vestibular recovery achieved in the *Ush1c* mutants after a single fetal dose of ASO-29 is surprising and may be associated with the timing of hair cell fate specification in the developing inner ear. Progenitors giving rise to auditory hair cells in the organ of Corti exit the cell cycle from ~E12-14 in a gradient beginning in the cochlear apex and progressing sequentially to the base (49–51). The proximity of the ASO-29 injection at E12.5 to the exit of hair cell progenitors from the cell cycle is anticipated to limit mitotic dilution of ASO-29 and support long-term retention of bioac-

tive levels of drug. Similarly, nascent vestibular hair cells begin to be specified prior to E12.5 when ASO-29 was injected (52), again mitigating the role of mitotic dilution. Once inside sensory cells, the fully-modified phosphorothioate backbone and 2′-*O*-methoxyethyl substitutions on sugars at all positions of ASO-29 further enhance intracellular stability and likely contribute to sustained bioactivity. The ASO-29 efficacy defined in our study is consistent with the stability and activity of ASO therapeutics in spinal muscular atrophy (SMA) patients treated intrathecally with ASO (53) and in treated non-human primates (54). Finally, our data dovetail with the ability of ASOs to ameliorate disease phenotypes for extended periods of time in animal models of SMA (55,56); spinocerebellar ataxia type 2 and type 3 (57,58); Huntington's disease (59); amyotrophic lateral sclerosis (60,61); Alzheimer's disease (62,63); nonalcoholic fatty liver disease (64); alpha-1 antitrypsin deficiency (65); autism-like disorder (66); and Angelman syndrome (67) as well as in our previous work with Usher syndrome (9).

The harmonin b isoform consists of 3 PDZ domains, 2 coiled-coiled domains, and a proline-serine-threonine (PST) rich domain (68,69). This scaffolding protein localizes to the upper tip link density of the stereocilium where the cadherin 23 (CDH23) component of the tip link inserts into the plasma membrane (22,70). Harmonin b interacts with CDH23 through its PDZ 2 domain and with F-actin through coiled-coiled and PST domains. It is unclear if harmonin, and attendant splicing correction of *Ush1c* pre-mRNA, is required only during stereociliary bundle morphogenesis to structure the upper tip link density or if *de novo* production of harmonin is also needed throughout life to maintain auditory and vestibular function. Importantly, harmonin b has been detected in mature mouse hair cells in the vicinity of the upper tip link density (70). Conditional deletion of harmonin at different stages of bundle morphogenesis and after hearing onset in juvenile and adult mice will further refine the timing and duration of harmonin expression required to maintain hearing and vestibular function.

Two previous gene replacement strategies targeting otic epithelial progenitors in mouse models of human hearing loss were effective in temporarily restoring inner ear function. Adeno-associated virus (AAV)-mediated gene transfer of methionine sulfoxide reductase B3 (*Msrb3*) into the E11.5 otocyst of the *Msrb3* knockout mouse restored 15% of the protein content and lowered ABR thresholds to wild type levels. Hearing in the treated *Msrb3* mutant deteriorated after four weeks of age as stereociliary bundle integrity was lost (71). Similarly, electroporation-mediated gene transfer of connexin 30 (*Cx30*) into the E11.5 otocyst of the *Cx30* knockout mouse restored auditory thresholds and endocochlear potential at P30 (72). The extent of the auditory recovery in the *Cx30* mutant beyond P30 was not reported (72). This work demonstrates that otic epithelial progenitors are a viable target for therapeutic intervention in a gene replacement context. The present study extends these findings demonstrating that otic progenitor targeting in the organ of Corti and nascent hair cell targeting in the vestibular sensory epithelia with a splice-switching ASO can modify intrinsic mRNA expression and lead to sustained recovery of sensory function into adulthood.

Identification of genetic mutations early during development is a prerequisite to enable fetal gene therapy for congenital deafness and vestibular dysfunction. By GA10, fetal DNA is present in sufficient quantity in maternal blood to enable detection of aneuploidies, sex-linked, and single gene mutations (73–79). Strategies to detect recessive and *de novo* mutations from cell-free fetal DNA are emerging as are approaches to first deduce and then screen the entire fetal genome (80,81). Advances in noninvasive prenatal testing will ensure that the molecular basis of mutations that cause congenital deafness and vestibular dysfunction in the neonate will be known with sufficient lead-time to intervene fetally (82–84).

Therapies administered to the developing inner ear *in utero* are expected to be influenced by variations in overall maternal and fetal health; the complexity of *in utero* drug delivery to the central and peripheral auditory systems; and the pharmacokinetics of ASO metabolism in the developing inner ear. It is therefore likely that the degree and the longevity of sensory rescue achieved with fetal inner ear therapeutics will be represented on a continuum with ASO-29-mediated splicing correction of *Ush1c c.216A* occupying one end of the spectrum. It is intriguing to consider an alternative, non-curative role for fetal therapeutics: to create a more receptive physiological environment in the inner ear for downstream, post-hearing therapeutic intervention that further augments sensory rescue. The recent hearing rescue achieved with dual AAV strategies to deliver otoferlin to inner hair cells of the otoferlin knockout mouse is predicated on the observation that affected inner hair cells remain structurally intact through P30 and are viable targets for functional rescue for an extended period of time (16,17). Fetal therapeutics may provide an opportunity to temporarily rescue sensory cells affected by deleterious genetic mutations that would otherwise cause cell death by birth, thus enabling adjuvant therapeutic engagement in these rescued cells postnatally. Ideally, these synergistic treatment paradigms would be tested in higher vertebrate model systems characterized by the fetal onset of hearing to closely model the developmental progression of human hearing.

Fetal gene therapeutics to treat neuronopathic Gaucher disease, beta thalassemia, tyrosinemia, and SMA have been defined in mouse models. An ASO with a similar chemistry to ASO-29 and targeted to increase exon inclusion in survival motor neuron 2 (SMN2) pre-mRNA in an animal model of SMA successfully improved SMN protein expression and ameliorated mutation-associated phenotypes in mice treated by intracerebroventricular injection into a lateral brain ventricle at E15 (55). AAV9-mediated gene transfer of glucocerebrosidase beta (GBA) to the E16 lateral ventricle of *Gba* mutant mice restored neuronal GBA expression, prevented neuronal degeneration, and mitigated neuroinflammation (85). Injection of peptide nucleic acid/DNA nanoparticles into the fetal vitelline vein at E15.5 edited a β-thalassemia-associated splice site mutation in intron 2 increasing hemoglobin concentrations at 6–10 weeks of age with improved red blood cell morphology, reduced splenic enlargement, and improved survival (86). Adenovirus-mediated transfer of base editor 3 targeting the 4-hydroxyphenylpyruvate dioxygenase gene in fumarylace-

toacetate hydrolase mutant mice rescued the lethal phenotype, and improved body weight and liver function without significant inflammation (87,88). In each of these diseases, fetal intervention either enhanced therapeutic outcomes or enabled postnatal survival.

In a compelling study validating human fetal therapy for X-linked hypohidrotic ectodermal dysplasia (XHED), ectodysplasin A-IgG1 fusion protein injected into the amniotic cavity of fetuses at GA26 and GA31 restored sweat-duct density, pilocarpine-induced sweating, improved eyelid meibomian-gland formation, and partially restored tooth germs (89). These data indicate that genetic mutations in the mammalian fetus are suitable targets for reparative gene therapies that effectively ameliorate disease phenotypes and, in the case of XHED, dramatically improve human health.

The translatability of fetal ASO pharmacotherapy for the treatment of congenital inner ear disease would likely be facilitated by dosing the amniotic cavity or other extra-embryonic target rather that engaging the embryo or fetal inner ear directly. The injection scheme deployed in the mouse otic vesicle at E12.5 suggests that the earlier delivery of ASO to otic progenitors and nascent vestibular hair cells is a critical parameter to achieve optimal therapeutic outcomes. Given the small volume of the amniotic cavity at early stages of inner ear development and the attendant challenges with drug retention, the mouse is not an ideal model system to further interrogate amniotic cavity or placental dosing strategies. We acknowledge a pressing need for higher vertebrate model systems with larger amniotic cavity volume that will enable testing of diverse dosing paradigms at different stages of inner ear development prior to the onset of hearing in order to fully assess pharmacotherapeutics to treat inner ear disease.

Our results demonstrate that an ASO pharmacotherapeutic administered to a developing organ system *in utero* corrects pre-mRNA splicing to preempt elaboration of the disease phenotype. We anticipate that fetal pharmacotherapeutics will become an essential tool for the treatment of congenital deafness and vestibular dysfunction given the precocious emergence of hearing in humans and the resistance of functionally mature hair cells to molecular correction. We conclude that the genetic modulation of the intrinsic reparative capacity of the developing fetus holds promise for improved management of intractable congenital diseases.

DATA AVAILABILITY

The authors declare that all the data supporting the findings of this study are available within the paper and its supplementary information files.

SUPPLEMENTARY DATA

Supplementary Data are available at NAR Online.

ACKNOWLEDGEMENTS

FUNDING

REFERENCES

1. Olusanya,B.O. (2012) Neonatal hearing screening and intervention in resource-limited settings: an overview. *Arch. Dis. Child.*, **97**, 654–659.
2. Shearer,A.E., Hildebrand,M.S. and Smith,R.J.H. (1993) In: Adam,MP, Ardinger,HH, Pagon,RA, Wallace,SE, Bean,LJH, Mefford,HC, Stephens,K, Amemiya,A and Ledbetter,N. (eds). GeneReviews®, Seattle (WA).
3. Akil,O., Seal,R.P., Burke,K., Wang,C., Alemi,A., During,M., Edwards,R.H. and Lustig,L.R. (2012) Restoration of hearing in the VGLUT3 knockout mouse using virally mediated gene therapy. *Neuron*, **75**, 283–293.
4. Askew,C., Rochat,C., Pan,B., Asai,Y., Ahmed,H., Child,E., Schneider,B.L., Aebischer,P. and Holt,J.R. (2015) Tmc gene therapy restores auditory function in deaf mice. *Sci. Transl. Med.*, **7**, 295ra108.
5. Gyorgy,B., Sage,C., Indzhykulian,A.A., Scheffer,D.I., Brisson,A.R., Tan,S., Wu,X., Volak,A., Mu,D., Tamvakologos,P.I. *et al.* (2017) Rescue of hearing by gene delivery to Inner-Ear hair cells using Exosome-Associated AAV. *Mol. Ther.*, **25**, 379–391.
6. Isgrig,K., Shteamer,J.W., Belyantseva,I.A., Drummond,M.C., Fitzgerald,T.S., Vijayakumar,S., Jones,S.M., Griffith,A.J., Friedman,T.B., Cunningham,L.L. *et al.* (2017) Gene therapy restores balance and auditory functions in a mouse model of Usher syndrome. *Mol. Ther.*, **25**, 780–791.
7. Pan,B., Askew,C., Galvin,A., Heman-Ackah,S., Asai,Y., Indzhykulian,A.A., Jodelka,F.M., Hastings,M.L., Lentz,J.J.,

Vandenberghe,L.H. *et al.* (2017) Gene therapy restores auditory and vestibular function in a mouse model of Usher syndrome type 1c. *Nat. Biotechnol.*, **35**, 264–272.

8. Emptoz,A., Michel,V., Lelli,A., Akil,O., Boutet de Monvel,J., Lahlou,G., Meyer,A., Dupont,T., Nouaille,S., Ey,E. *et al.* (2017) Local gene therapy durably restores vestibular function in a mouse model of Usher syndrome type 1G. *Proc. Natl. Acad. Sci. U.S.A.*, **114**, 9695–9700.

9. Lentz,J.J., Jodelka,F.M., Hinrich,A.J., McCaffrey,K.E., Farris,H.E., Spalitta,M.J., Bazan,N.G., Duelli,D.M., Rigo,F. and Hastings,M.L. (2013) Rescue of hearing and vestibular function by antisense oligonucleotides in a mouse model of human deafness. *Nat. Med.*, **19**, 345–350.

10. Ponnath,A., Depreux,F.F., Jodelka,F.M., Rigo,F., Farris,H.E., Hastings,M.L. and Lentz,J.J. (2018) Rescue of outer hair cells with antisense oligonucleotides in usher mice is dependent on age of treatment. *J. Assoc. Res. Otolaryngol.*, **19**, 1–16.

11. Gao,X., Tao,Y., Lamas,V., Huang,M., Yeh,W.H., Pan,B., Hu,Y.J., Hu,J.H., Thompson,D.B., Shu,Y. *et al.* (2018) Treatment of autosomal dominant hearing loss by in vivo delivery of genome editing agents. *Nature*, **553**, 217–221.

12. Shibata,S.B., Ranum,P.T., Moteki,H., Pan,B., Goodwin,A.T., Goodman,S.S., Abbas,P.J., Holt,J.R. and Smith,R.J.H. (2016) RNA interference prevents autosomal-dominant hearing loss. *Am. J. Hum. Genet.*, **98**, 1101–1113.

13. Alagramam,K.N., Gopal,S.R., Geng,R., Chen,D.H., Nemet,I., Lee,R., Tian,G., Miyagi,M., Malagu,K.F., Lock,C.J. *et al.* (2016) A small molecule mitigates hearing loss in a mouse model of Usher syndrome III. *Nat. Chem. Biol.*, **12**, 444–451.

14. Dulon,D., Papal,S., Patni,P., Cortese,M., Vincent,P.F., Tertrais,M., Emptoz,A., Tlili,A., Bouleau,Y., Michel,V. *et al.* (2018) Clarin-1 gene transfer rescues auditory synaptopathy in model of Usher syndrome. *J. Clin. Invest.*, **128**, 3382–3401.

15. Nakano,Y., Kelly,M.C., Rehman,A.U., Boger,E.T., Morell,R.J., Kelley,M.W., Friedman,T.B. and Banfi,B. (2018) Defects in the alternative splicing-dependent regulation of REST cause deafness. *Cell*, **174**, 536–548.

16. Akil,O., Dyka,F., Calvet,C., Emptoz,A., Lahlou,G., Nouaille,S., Boutet de Monvel,J., Hardelin,J.P., Hauswirth,W.W., Avan,P. *et al.* (2019) Dual AAV-mediated gene therapy restores hearing in a DFNB9 mouse model. *Proc. Natl. Acad. Sci. U.S.A.*, **116**, 4496–4501.

17. Al-Moyed,H., Cepeda,A.P., Jung,S., Moser,T., Kugler,S. and Reisinger,E. (2019) A dual-AAV approach restores fast exocytosis and partially rescues auditory function in deaf otoferlin knock-out mice. *EMBO Mol. Med.*, **11**, 1–13.

18. Millan,J.M., Aller,E., Jaijo,T., Blanco-Kelly,F., Gimenez-Pardo,A. and Ayuso,C. (2011) An update on the genetics of usher syndrome. *J. Ophthalmol.*, **2011**, 417217.

19. Lentz,J. and Keats,B.J.B. (1993) In: Adam,MP, Ardinger,HH, Pagon,RA, Wallace,SE, Bean,LJH, Stephens,K and Amemiya,A (eds). GeneReviews®, Seattle (WA).

20. Qiu,X. and Muller,U. (2018) Mechanically gated Ion channels in mammalian hair cells. *Front. Cell Neurosci.*, **12**, 100.

21. Gregory,F.D., Bryan,K.E., Pangrsic,T., Calin-Jageman,I.E., Moser,T. and Lee,A. (2011) Harmonin inhibits presynaptic Cav1.3 Ca(2)(+) channels in mouse inner hair cells. *Nat. Neurosci.*, **14**, 1109–1111.

22. Grillet,N., Xiong,W., Reynolds,A., Kazmierczak,P., Sato,T., Lillo,C., Dumont,R.A., Hintermann,E., Sczaniecka,A., Schwander,M. *et al.* (2009) Harmonin mutations cause mechanotransduction defects in cochlear hair cells. *Neuron*, **62**, 375–387.

23. Gregory,F.D., Pangrsic,T., Calin-Jageman,I.E., Moser,T. and Lee,A. (2013) Harmonin enhances voltage-dependent facilitation of Cav1.3 channels and synchronous exocytosis in mouse inner hair cells. *J. Physiol.*, **591**, 3253–3269.

24. Lentz,J., Pan,F., Ng,S.S., Deininger,P. and Keats,B. (2007) Ush1c216A knock-in mouse survives Katrina. *Mutat. Res.*, **616**, 139–144.

25. Lentz,J.J., Gordon,W.C., Farris,H.E., MacDonald,G.H., Cunningham,D.E., Robbins,C.A., Tempel,B.L., Bazan,N.G., Rubel,E.W., Oesterle,E.C. *et al.* (2010) Deafness and retinal degeneration in a novel USH1C knock-in mouse model. *Dev. Neurobiol.*, **70**, 253–267.

26. Bennett,C.F. (2019) Therapeutic antisense oligonucleotides are coming of age. *Annu. Rev. Med.*, **70**, 307–321.

27. Hastings,M.L. and Jones,T.A. (2019) Antisense oligonucleotides for the treatment of inner ear dysfunction. *Neurotherapeutics*, **16**, 348–359.

28. Vijayakumar,S., Depreux,F.F., Jodelka,F.M., Lentz,J.J., Rigo,F., Jones,T.A. and Hastings,M.L. (2017) Rescue of peripheral vestibular function in Usher syndrome mice using a splice-switching antisense oligonucleotide. *Hum. Mol. Genet.*, **26**, 3482–3494.

29. Hepper,P.G. and Shahidullah,B.S. (1994) Development of fetal hearing. *Arch. Dis. Child.*, **71**, F81–F87.

30. Locher,H., Frijns,J.H., van Iperen,L., de Groot,J.C., Huisman,M.A. and Chuva de Sousa Lopes,S.M. (2013) Neurosensory development and cell fate determination in the human cochlea. *Neural Dev.*, **8**, 20.

31. Wang,L., Kempton,J.B. and Brigande,J.V. (2018) Gene therapy in mouse models of deafness and balance dysfunction. *Front. Mol. Neurosci.*, **11**, 300.

32. Depreux,F.F., Wang,L., Jiang,H., Jodelka,F.M., Rosencrans,R.F., Rigo,F., Lentz,J.J., Brigande,J.V. and Hastings,M.L. (2016) Antisense oligonucleotides delivered to the amniotic cavity in utero modulate gene expression in the postnatal mouse. *Nucleic Acids Res.*, **44**, 9519–9529.

33. National Research Council (U.S.) (2011) In: *Committee for the Update of the Guide for the Care and Use of Laboratory Animals., Institute for Laboratory Animal Research (U.S.) and National Academies Press (U.S.)*. 8th ed. National Academies Press, Washington, D.C., pp. xxv, 220 p.

34. Wang,L., Jiang,H. and Brigande,J.V. (2012) Gene transfer to the developing mouse inner ear by in vivo electroporation. *J. Vis. Exp.*, **64**, e3653.

35. Beurg,M., Xiong,W., Zhao,B., Muller,U. and Fettiplace,R. (2015) Subunit determination of the conductance of hair-cell mechanotransducer channels. *Proc. Natl. Acad. Sci. U.S.A.*, **112**, 1589–1594.

36. Schneider,C.A., Rasband,W.S. and Eliceiri,K.W. (2012) NIH Image to ImageJ: 25 years of image analysis. *Nat. Methods*, **9**, 671–675.

37. Tateya,T., Imayoshi,I., Tateya,I., Hamaguchi,K., Torii,H., Ito,J. and Kageyama,R. (2013) Hedgehog signaling regulates prosensory cell properties during the basal-to-apical wave of hair cell differentiation in the mammalian cochlea. *Development*, **140**, 3848–3857.

38. Muller,M., von Hunerbein,K., Hoidis,S. and Smolders,J.W. (2005) A physiological place-frequency map of the cochlea in the CBA/J mouse. *Hear. Res.*, **202**, 63–73.

39. Ebrahim,S., Avenarius,M.R., Grati,M., Krey,J.F., Windsor,A.M., Sousa,A.D., Ballesteros,A., Cui,R., Millis,B.A., Salles,F.T. *et al.* (2016) Stereocilia-staircase spacing is influenced by myosin III motors and their cargos espin-1 and espin-like. *Nat. Commun.*, **7**, 10833.

40. Self,T., Mahony,M., Fleming,J., Walsh,J., Brown,S.D. and Steel,K.P. (1998) Shaker-1 mutations reveal roles for myosin VIIA in both development and function of cochlear hair cells. *Development*, **125**, 557–566.

41. Carter,R.J., Morton,J. and Dunnett,S.B. (2001) Motor coordination and balance in rodents. *Curr. Protoc. Neurosci.*, doi:10.1002/0471142301.ns0812s15.

42. Goodyear,R.J., Jones,S.M., Sharifi,L., Forge,A. and Richardson,G.P. (2012) Hair bundle defects and loss of function in the vestibular end organs of mice lacking the receptor-like inositol lipid phosphatase PTPRQ. *J. Neurosci.*, **32**, 2762–2772.

43. Hardisty-Hughes,R.E., Parker,A. and Brown,S.D. (2010) A hearing and vestibular phenotyping pipeline to identify mouse mutants with hearing impairment. *Nat. Protoc.*, **5**, 177–190.

44. Soucy,N.V., Riley,J.P., Templin,M.V., Geary,R., de Peyster,A. and Levin,A.A. (2006) Maternal and fetal distribution of a phosphorothioate oligonucleotide in rats after intravenous infusion. *Birth Defects Res. B Dev. Reprod. Toxicol.*, **77**, 22–28.

45. Bok,J., Chang,W. and Wu,D.K. (2007) Patterning and morphogenesis of the vertebrate inner ear. *Int. J. Dev. Biol.*, **51**, 521–533.

46. Riccomagno,M.M., Martinu,L., Mulheisen,M., Wu,D.K. and Epstein,D.J. (2002) Specification of the mammalian cochlea is dependent on Sonic hedgehog. *Genes Dev.*, **16**, 2365–2378.

47. Gubbels,S.P., Woessner,D.W., Mitchell,J.C., Ricci,A.J. and Brigande,J.V. (2008) Functional auditory hair cells produced in the mammalian cochlea by in utero gene transfer. *Nature*, **455**, 537–541.

48. Ren,T. (2004) Reverse propagation of sound in the gerbil cochlea. *Nat. Neurosci.*, **7**, 333–334.

49. Chen,P. and Segil,N. (1999) p27(Kip1) links cell proliferation to morphogenesis in the developing organ of Corti. *Development*, **126**, 1581–1590.

50. Lee,Y.S., Liu,F. and Segil,N. (2006) A morphogenetic wave of p27Kip1 transcription directs cell cycle exit during organ of Corti development. *Development*, **133**, 2817–2826.

51. Prajapati-DiNubila,M., Benito-Gonzalez,A., Golden,E.J., Zhang,S. and Doetzlhofer,A. (2019) A counter gradient of Activin A and follistatin instructs the timing of hair cell differentiation in the murine cochlea. *Elife*, **8**, e47613.

52. Bermingham,N.A., Hassan,B.A., Price,S.D., Vollrath,M.A., Ben-Arie,N., Eatock,R.A., Bellen,H.J., Lysakowski,A. and Zoghbi,H.Y. (1999) Math1: an essential gene for the generation of inner ear hair cells. *Science*, **284**, 1837–1841.

53. Ramos,D.M., d'Ydewalle,C., Gabbeta,V., Dakka,A., Klein,S.K., Norris,D.A., Matson,J., Taylor,S.J., Zaworski,P.G., Prior,T.W. *et al.* (2019) Age-dependent SMN expression in disease-relevant tissue and implications for SMA treatment. *J. Clin. Invest.*, **129**, 4817–4831.

54. Rigo,F., Chun,S.J., Norris,D.A., Hung,G., Lee,S., Matson,J., Fey,R.A., Gaus,H., Hua,Y., Grundy,J.S. *et al.* (2014) Pharmacology of a central nervous system delivered 2′-O-methoxyethyl-modified survival of motor neuron splicing oligonucleotide in mice and nonhuman primates. *J. Pharmacol. Exp. Ther.*, **350**, 46–55.

55. Hua,Y., Sahashi,K., Rigo,F., Hung,G., Horev,G., Bennett,C.F. and Krainer,A.R. (2011) Peripheral SMN restoration is essential for long-term rescue of a severe spinal muscular atrophy mouse model. *Nature*, **478**, 123–126.

56. Passini,M.A., Bu,J., Richards,A.M., Kinnecom,C., Sardi,S.P., Stanek,L.M., Hua,Y., Rigo,F., Matson,J., Hung,G. *et al.* (2011) Antisense oligonucleotides delivered to the mouse CNS ameliorate symptoms of severe spinal muscular atrophy. *Sci. Transl. Med.*, **3**, 72ra18.

57. Scoles,D.R., Meera,P., Schneider,M.D., Paul,S., Dansithong,W., Figueroa,K.P., Hung,G., Rigo,F., Bennett,C.F., Otis,T.S. *et al.* (2017) Antisense oligonucleotide therapy for spinocerebellar ataxia type 2. *Nature*, **544**, 362–366.

58. McLoughlin,H.S., Moore,L.R., Chopra,R., Komlo,R., McKenzie,M., Blumenstein,K.G., Zhao,H., Kordasiewicz,H.B., Shakkottai,V.G. and Paulson,H.L. (2018) Oligonucleotide therapy mitigates disease in spinocerebellar ataxia type 3 mice. *Ann. Neurol.*, **84**, 64–77.

59. Southwell,A.L., Kordasiewicz,H.B., Langbehn,D., Skotte,N.H., Parsons,M.P., Villanueva,E.B., Caron,N.S., Ostergaard,M.E., Anderson,L.M., Xie,Y. *et al.* (2018) Huntingtin suppression restores cognitive function in a mouse model of Huntington's disease. *Sci. Transl. Med.*, **10**, eaar3959.

60. Becker,L.A., Huang,B., Bieri,G., Ma,R., Knowles,D.A., Jafar-Nejad,P., Messing,J., Kim,H.J., Soriano,A., Auburger,G. *et al.* (2017) Therapeutic reduction of ataxin-2 extends lifespan and reduces pathology in TDP-43 mice. *Nature*, **544**, 367–371.

61. Smith,R.A., Miller,T.M., Yamanaka,K., Monia,B.P., Condon,T.P., Hung,G., Lobsiger,C.S., Ward,C.M., McAlonis-Downes,M., Wei,H. *et al.* (2006) Antisense oligonucleotide therapy for neurodegenerative disease. *J. Clin. Invest.*, **116**, 2290–2296.

62. DeVos,S.L., Miller,R.L., Schoch,K.M., Holmes,B.B., Kebodeaux,C.S., Wegener,A.J., Chen,G., Shen,T., Tran,H., Nichols,B. *et al.* (2017) Tau reduction prevents neuronal loss and reverses pathological tau deposition and seeding in mice with tauopathy. *Sci. Transl. Med.*, **9**, eaag0481.

63. Hinrich,A.J., Jodelka,F.M., Chang,J.L., Brutman,D., Bruno,A.M., Briggs,C.A., James,B.D., Stutzmann,G.E., Bennett,D.A., Miller,S.A. *et al.* (2016) Therapeutic correction of ApoER2 splicing in Alzheimer's disease mice using antisense oligonucleotides. *EMBO Mol. Med.*, **8**, 328–345.

64. Cansby,E., Nunez-Duran,E., Magnusson,E., Amrutkar,M., Booten,S.L., Kulkarni,N.M., Svensson,L.T., Boren,J., Marschall,H.U., Aghajan,M. *et al.* (2019) Targeted delivery of Stk25 antisense oligonucleotides to hepatocytes protects mice against nonalcoholic fatty liver disease. *Cell. Mol. Gastroenterol. Hepatol.*, **7**, 597–618.

65. Guo,S., Booten,S.L., Aghajan,M., Hung,G., Zhao,C., Blomenkamp,K., Gattis,D., Watt,A., Freier,S.M., Teckman,J.H. *et al.* (2014) Antisense oligonucleotide treatment ameliorates alpha-1 antitrypsin-related liver disease in mice. *J. Clin. Invest.*, **124**, 251–261.

66. Sztainberg,Y., Chen,H.M., Swann,J.W., Hao,S., Tang,B., Wu,Z., Tang,J., Wan,Y.W., Liu,Z., Rigo,F. *et al.* (2015) Reversal of phenotypes in MECP2 duplication mice using genetic rescue or antisense oligonucleotides. *Nature*, **528**, 123–126.

67. Meng,L., Ward,A.J., Chun,S., Bennett,C.F., Beaudet,A.L. and Rigo,F. (2015) Towards a therapy for Angelman syndrome by targeting a long non-coding RNA. *Nature*, **518**, 409–412.

68. Verpy,E., Leibovici,M., Zwaenepoel,I., Liu,X.Z., Gal,A., Salem,N., Mansour,A., Blanchard,S., Kobayashi,I., Keats,B.J. *et al.* (2000) A defect in harmonin, a PDZ domain-containing protein expressed in the inner ear sensory hair cells, underlies Usher syndrome type 1C. *Nat. Genet.*, **26**, 51–55.

69. Boeda,B., El-Amraoui,A., Bahloul,A., Goodyear,R., Daviet,L., Blanchard,S., Perfettini,I., Fath,K.R., Shorte,S., Reiners,J. *et al.* (2002) Myosin VIIa, harmonin and cadherin 23, three Usher I gene products that cooperate to shape the sensory hair cell bundle. *EMBO J.*, **21**, 6689–6699.

70. Lefevre,G., Michel,V., Weil,D., Lepelletier,L., Bizard,E., Wolfrum,U., Hardelin,J.P. and Petit,C. (2008) A core cochlear phenotype in USH1 mouse mutants implicates fibrous links of the hair bundle in its cohesion, orientation and differential growth. *Development*, **135**, 1427–1437.

71. Kim,M.A., Cho,H.J., Bae,S.H., Lee,B., Oh,S.K., Kwon,T.J., Ryoo,Z.Y., Kim,H.Y., Cho,J.H., Kim,U.K. *et al.* (2016) Methionine sulfoxide reductase B3-Targeted in utero gene therapy rescues hearing function in a mouse model of congenital sensorineural hearing loss. *Antioxid. Redox. Signal.*, **24**, 590–602.

72. Miwa,T., Minoda,R., Ise,M., Yamada,T. and Yumoto,E. (2013) Mouse otocyst transuterine gene transfer restores hearing in mice with connexin 30 deletion-associated hearing loss. *Mol. Ther.*, **21**, 1142–1150.

73. Chiu,R.W., Akolekar,R., Zheng,Y.W., Leung,T.Y., Sun,H., Chan,K.C., Lun,F.M., Go,A.T., Lau,E.T., To,W.W. *et al.* (2011) Non-invasive prenatal assessment of trisomy 21 by multiplexed maternal plasma DNA sequencing: large scale validity study. *BMJ*, **342**, c7401.

74. Chiu,R.W., Chan,K.C., Gao,Y., Lau,V.Y., Zheng,W., Leung,T.Y., Foo,C.H., Xie,B., Tsui,N.B., Lun,F.M. *et al.* (2008) Noninvasive prenatal diagnosis of fetal chromosomal aneuploidy by massively parallel genomic sequencing of DNA in maternal plasma. *Proc. Natl. Acad. Sci. U.S.A.*, **105**, 20458–20463.

75. Fan,H.C., Gu,W., Wang,J., Blumenfeld,Y.J., El-Sayed,Y.Y. and Quake,S.R. (2012) Non-invasive prenatal measurement of the fetal genome. *Nature*, **487**, 320–324.

76. Kitzman,J.O., Snyder,M.W., Ventura,M., Lewis,A.P., Qiu,R., Simmons,L.E., Gammill,H.S., Rubens,C.E., Santillan,D.A., Murray,J.C. *et al.* (2012) Noninvasive whole-genome sequencing of a human fetus. *Sci. Transl. Med.*, **4**, 137ra176.

77. Lam,K.W., Jiang,P., Liao,G.J., Chan,K.C., Leung,T.Y., Chiu,R.W. and Lo,Y.M. (2012) Noninvasive prenatal diagnosis of monogenic diseases by targeted massively parallel sequencing of maternal plasma: application to beta-thalassemia. *Clin. Chem.*, **58**, 1467–1475.

78. Lo,Y.M., Corbetta,N., Chamberlain,P.F., Rai,V., Sargent,I.L., Redman,C.W. and Wainscoat,J.S. (1997) Presence of fetal DNA in maternal plasma and serum. *Lancet*, **350**, 485–487.

79. Srinivasan,A., Bianchi,D.W., Huang,H., Sehnert,A.J. and Rava,R.P. (2013) Noninvasive detection of fetal subchromosome abnormalities via deep sequencing of maternal plasma. *Am. J. Hum. Genet.*, **92**, 167–176.

80. Chan,K.C., Jiang,P., Sun,K., Cheng,Y.K., Tong,Y.K., Cheng,S.H., Wong,A.I., Hudecova,I., Leung,T.Y., Chiu,R.W. *et al.* (2016) Second generation noninvasive fetal genome analysis reveals de novo mutations, single-base parental inheritance, and preferred DNA ends. *Proc. Natl. Acad. Sci. U.S.A.*, **113**, E8159–E8168.

81. Zeevi,D.A., Altarescu,G., Weinberg-Shukron,A., Zahdeh,F., Dinur,T., Chicco,G., Herskovitz,Y., Renbaum,P., Elstein,D., Levy-Lahad,E. *et al.* (2015) Proof-of-principle rapid noninvasive prenatal diagnosis of autosomal recessive founder mutations. *J. Clin. Invest.*, **125**, 3757–3765.

82. Bianchi,D.W. and Chiu,R.W.K. (2018) Sequencing of circulating Cell-free DNA during pregnancy. *N. Engl. J. Med.*, **379**, 464–473.

83. Vermeesch,J.R., Voet,T. and Devriendt,K. (2016) Prenatal and pre-implantation genetic diagnosis. *Nat. Rev. Genet.*, **17**, 643–656.

84. Jelin,A.C., Sagaser,K.G. and Wilkins-Haug,L. (2019) Prenatal genetic testing options. *Pediatr. Clin. North Am.*, **66**, 281–293.

85. Massaro,G., Mattar,C.N.Z., Wong,A.M.S., Sirka,E., Buckley,S.M.K., Herbert,B.R., Karlsson,S., Perocheau,D.P., Burke,D. *et al.* (2018) Fetal gene therapy for neurodegenerative disease of infants. *Nat. Med.*, **24**, 1317–1323.

86. Ricciardi,A.S., Bahal,R., Farrelly,J.S., Quijano,E., Bianchi,A.H., Luks,V.L., Putman,R., Lopez-Giraldez,F., Coskun,S., Song,E. *et al.* (2018) In utero nanoparticle delivery for site-specific genome editing. *Nat. Commun.*, **9**, 2481.

87. Rossidis,A.C., Stratigis,J.D., Chadwick,A.C., Hartman,H.A., Ahn,N.J., Li,H., Singh,K., Coons,B.E., Li,L., Lv,W. *et al.* (2018) In utero CRISPR-mediated therapeutic editing of metabolic genes. *Nat. Med.*, **24**, 1513–1518.

88. Rees,H.A. and Liu,D.R. (2018) Base editing: precision chemistry on the genome and transcriptome of living cells. *Nat. Rev. Genet.*, **19**, 770–788.

89. Schneider,H., Faschingbauer,F., Schuepbach-Mallepell,S., Korber,I., Wohlfart,S., Dick,A., Wahlbuhl,M., Kowalczyk-Quintas,C., Vigolo,M., Kirby,N. *et al.* (2018) Prenatal correction of X-Linked hypohidrotic ectodermal dysplasia. *N. Engl. J. Med.*, **378**, 1604–1610.

90. Shnerson,A. and Willott,J.F. (1980) Ontogeny of the acoustic startle response in C57BL/6J mouse pups. *J. Comp. Physiol. Psychol.*, **94**, 36–40.